

Asymmetry of Atmospheric Circulation Anomalies over the Western North Pacific between El Niño and La Niña*

BO WU

LASG, Institute of Atmospheric Physics, Chinese Academy of Sciences, and Graduate University of Chinese Academy of Sciences, Beijing, China

TIM LI

IPRC, and Department of Meteorology, University of Hawaii at Manoa, Honolulu, Hawaii

TIANJUN ZHOU

LASG, Institute of Atmospheric Physics, Chinese Academy of Sciences, Beijing, China

(Manuscript received 27 April 2009, in final form 26 January 2010)

ABSTRACT

The asymmetry of the western North Pacific (WNP) low-level atmospheric circulation anomalies between the El Niño and La Niña mature winter is examined. An anomalous WNP cyclone (WNPC) center during La Niña tends to shift westward relative to an anomalous WNP anticyclone (WNPAC) center during El Niño. Two factors may contribute to this asymmetric response. The first factor is the longitudinal shifting of El Niño and La Niña anomalous heating. The composite negative precipitation anomaly center during La Niña is located farther to the west of the composite positive precipitation anomaly center during El Niño. The westward shift of the heating may further push the WNPC westward relative to the position of the WNPAC. The second factor is the amplitude asymmetry of sea surface temperature anomalies (SSTAs) in the WNP, namely, the amplitude of local cold SSTA during El Niño is greater than that of warm SSTA during La Niña. The asymmetry of SSTA is originated from the asymmetric SSTA tendencies during the ENSO developing summer. Although both precipitation and surface wind anomalies are approximately symmetric, the surface latent heat flux anomalies are highly asymmetric over the key WNP region, where the climate mean zonal wind speed is small. Both the anomalous westerly during El Niño and the anomalous easterly during La Niña in the region lead to an enhanced surface evaporation, strengthening (weakening) the enhancement of the cold (warm) SSTA in situ during El Niño (La Niña). The asymmetry of the SSTA in the WNP is further amplified due to anomalous wind differences between El Niño and La Niña in their mature winter. Atmospheric general circulation model experiments demonstrate that both factors contribute to the asymmetry between the WNPAC and WNPC. The asymmetric circulation in the WNP contributes to the asymmetry of temporal evolutions between El Niño and La Niña.

1. Introduction

During the mature phase of El Niño, the most prominent low-level atmospheric circulation anomalies over

the tropical western Pacific and East Asia is an off-equatorial anomalous anticyclone [hereafter the western North Pacific (WNP) anticyclone (WNPAC)] (Wang et al. 2000; Chang et al. 2000a). The WNPAC is a key bridge that links El Niño and the East Asian summer monsoon (Chang et al. 2000a,b; Wang et al. 2000; Wu et al. 2003). It influences the East Asian climate from the El Niño mature winter to the following summer. Concurring with the formation of the WNPAC, a positive anomalous rainfall belt extends from southeastern China to the Kuroshio Extension region in boreal winter and spring owing to anomalous moisture transport by the southerly component in the northwestern flank of the WNPAC (Zhang

* School of Ocean and Earth Science and Technology Contribution Number 7907 and International Pacific Research Center Contribution Number 683.

Corresponding author address: Dr. Tianjun Zhou, LASG, Institute of Atmospheric Physics, Chinese Academy of Sciences, Beijing 100029, China.
E-mail: zhoutj@lasg.iap.ac.cn

et al. 1996; Lau and Nath 2000; Zhang and Sumi 2002). During the subsequent summer, the WNPAC favors a westward extension of the western Pacific subtropical high, which blocks the mei-yu front from moving southward and thereby prolongs the frontal rainfall along the lower reaches of the Yangtze River and the Huaihe River valleys (Chang et al. 2000a,b; Zhou and Yu 2005; Sui et al. 2007; Wu and Zhou 2008).

As a response to El Niño forcing, the WNPAC may play a role in the phase reversal of El Niño (Wang et al. 2001). Easterly anomalies to the south of the WNPAC may stimulate oceanic upwelling Kelvin waves and thus reverse warm SST anomalies (SSTAs) in the equatorial central-eastern Pacific (Weisberg and Wang 1997a,b; Wang et al. 1999a; Kim and Lau 2001; Li et al. 2007; Ohba and Ueda 2009).

The WNPAC is tightly coupled with underlying ocean surface cooling. The northeasterly anomalies over the southeastern flank of the WNPAC increase the background mean northeasterly trades and generate a colder SST in situ through enhanced evaporation. The negative SSTAs further suppress convection and stimulate a descending Rossby wave to the northwest and thus reinforce the WNPAC (Wang et al. 2003). This positive wind–evaporation–SST feedback maintains the WNPAC through the El Niño mature winter and the subsequent spring (Wang et al. 2000). The “wind–evaporation–SST” feedback was first proposed to study the equatorial asymmetry of the intertropical convergence zone (Xie and Philander 1994; Li 1997), and then was used to study the decadal variability over the tropical Atlantic (Chang et al. 1997; Xie 1999) and the phase locking of ENSO (Wang et al. 1999b). In the study, we will explore the nonlinear feature of the wind–evaporation process over the western North Pacific.

While the WNPAC is maintained by local air–sea interaction, it is initiated possibly through the following three routes. First, circulation anomalies in response to the El Niño heating over the equatorial central Pacific generate cold SSTAs in the western Pacific, which further set up the WNPAC (Wang et al. 2000). Second, the deepening of the East Asian trough and the intrusion of midlatitude cold air into the Philippine Sea might trigger the WNPAC (Wang and Zhang 2002; Lau and Nath 2006). Third, the WNPAC results from the eastward movement of an anomalous anticyclone established over the northern Indian Ocean (Chou 2004; Chen et al. 2007).

Most previous studies assumed a symmetric circulation feature between El Niño and La Niña; namely, there is an anomalous anticyclone (cyclone) over the WNP during the El Niño (La Niña) mature winter. However, it is important to note that El Niño and La Niña

have a significant asymmetry in amplitude, structure, and temporal evolution (e.g., Hoerling et al. 1997; Burgers and Stephenson 1999; Kang and Kug 2002; Jin et al. 2003; An and Jin 2004; An et al. 2005). The anomalous convection over the equatorial central Pacific during La Niña tends to shift to the west of its El Niño counterpart (Hoerling et al. 1997). Numerical model experiments indicated that this asymmetry is attributed to nonlinear atmospheric responses to the underlying SSTA (Hoerling et al. 1997; Kang and Kug 2002).

The anomalous convective heating over the equatorial central Pacific is a crucial factor that impacts the circulation over the WNP (Lau and Nath 2000; Wu and Zhou 2008; Zhou et al. 2009a,b). Given the asymmetric SSTA pattern between El Niño and La Niña, one may wonder whether the WNP atmospheric response to El Niño and La Niña is asymmetric. In this paper, we attempt to address the following questions: 1) are WNPAC and WNP cyclone (WNPC) during the El Niño and La Niña mature winter asymmetric and 2), If they show an asymmetric characteristic, what are the physical mechanisms that cause the asymmetry?

The rest of the paper is organized as follows. Datasets, analysis methods, and an atmospheric general circulation model (AGCM) are described in section 2. Section 3 presents the asymmetric circulation features over the WNP between El Niño and La Niña. In section 4, we discuss two possible factors that cause the asymmetry. The two factors are further examined through a series of AGCM numerical experiments in section 5. The impacts of the asymmetry on ENSO evolution are discussed in section 6. Summary and concluding remarks are given in section 7.

2. Data, method, and model experiments

a. Data and method

The datasets used in the present study consist of 1) the 850-hPa and 1000-hPa wind fields and the surface heat flux from the National Centers for Environment Prediction–National Center for Atmospheric Research (NCEP–NCAR) reanalysis data (Kalnay et al. 1996) for the period from 1948 to 2004, 2) SST data from the Hadley Centre Global Sea Ice and Sea Surface Temperature dataset (HadISST) (Rayner et al. 2003) for the period 1948–2004, 3) monthly precipitation anomalies over global land and oceans for the same period from the precipitation reconstruction (PREC) dataset (Chen et al. 2002), and 4) oceanic subsurface temperature data from a simple ocean data assimilation analysis of global upper ocean (SODA) (Carton et al. 2000) for the period from 1950 to 2000.

TABLE 1. El Niño and La Niña events in the period of 1949–2002, used in the study.

El Niño	1957, 1965, 1972, 1982, 1986, 1991, 1994, 1997, 2002
La Niña	1949, 1955, 1970, 1973, 1975, 1984, 1988, 1998, 1999

A composite analysis method is applied. We chose nine El Niño events and nine La Niña events in the period 1948–2002. The selection of El Niño and La Niña events is based on the threshold of one standard deviation of wintertime [December–February (DJF)] mean Niño-3.4 index, which is defined as the area-averaged SSTA over the region 5°N–5°S, 120°–170°W. The selected ENSO years are listed in Table 1.

To focus on the interannual time scale, variations longer than 8 years are filtered out from the original datasets with a Lanczos filter (Duchon 1979). Following Hoerling et al. (1997), the difference between the composite El Niño and La Niña events is regarded as a symmetric component, and the sum of them is regarded as an asymmetric component.

b. Model description and experiment design

The AGCM used in the study is the ECHAM version 4.6 (ECHAM4) developed by the Max Planck Institute for Meteorology (Roeckner et al. 1996). The model was run at a horizontal resolution of spectral triangular 42 (T42), roughly equivalent to 2.8° latitude × 2.8° longitude, with 19 vertical levels in a hybrid sigma pressure-coordinate system extending from the surface to 10 hPa. The SST data used as the lower boundary condition is the same as that used in the observational analysis.

As listed in Table 2, four sets of model experiments are designed:

- 1) Control run (CTRL run): the ECHAM4 was integrated for 10 years, forced by monthly climatological SST based on the period 1948–2005.
- 2) Global SSTA forcing runs for El Niño and La Niña: composite El Niño or La Niña SSTA was added to

the climatological SST in the global ocean (GB experiment); the run with SSTA derived from El Niño (La Niña) is referred to as the GBEL (GBLA) run.

- 3) Tropical central-eastern Pacific SSTA forcing runs for El Niño and La Niña: These experiments were the same as the GB experiments except that only the positive (negative) SSTA in the tropical central-eastern Pacific (CE experiment) associated with El Niño (La Niña) was added to the climatological mean SST field. The runs with SSTA derived from El Niño (La Niña) are referred to as CEEL (CELA) runs.
- 4) Western North Pacific SSTA forcing runs for El Niño and La Niña: the experiments were the same as the GB experiments except that only the negative (positive) SSTA in the western North Pacific (WP experiment) associated with El Niño (La Niña) was added to the climatological mean SST field. The runs with SSTA derived from El Niño (La Niña) are referred to as WPEL (WPLA) runs.

For each sets of experiment, an ensemble simulation with 10 members was performed. Among the 10 members, each realization only differed in initial condition but was forced by an identical SST field. The model was integrated from October to February in each simulation. The ensemble mean of December–February is analyzed.

3. Asymmetry of circulation anomalies between El Niño and La Niña

The composite 850-hPa streamfunction anomalies during the mature phase (DJF) of El Niño and La Niña are shown in Figs. 1a,b. In the El Niño composite, an off-equatorial anomalous anticyclone is evident over the WNP, with a center located in the Philippine Sea. The anomalous easterlies in the southern flank of the anticyclone extend eastward to 155°E. Twin cyclone couplets straddle over the central equatorial Pacific, accompanied with westerly anomalies on the equator. In contrast, in the La Niña composite the northern branch of the twin anticyclone couplets over the central equatorial Pacific

TABLE 2. List of numerical experiments.

Expt	SST forcing field	Integration
CTRL	Global climatological SST	10 years
GBEL and GBLA	Add the composite SSTAs to the climatological SST of the global ocean	10 realizations for both GBEL and GBLA
CEEL and CELA	Add the composite positive (negative) SSTAs in the tropical central-eastern Pacific (160°E–100°W, 30°S–30°N) to the climatological SST in CEEL (CELA)	10 realizations for both CEEL and CELA
WPEL and WPLA	Add the composite negative (positive) SSTAs in the WNP (120°–160°E, 0°–20°N) to the climatological SST in WPEL (WPLA)	10 realizations for both WPEL and WPLA

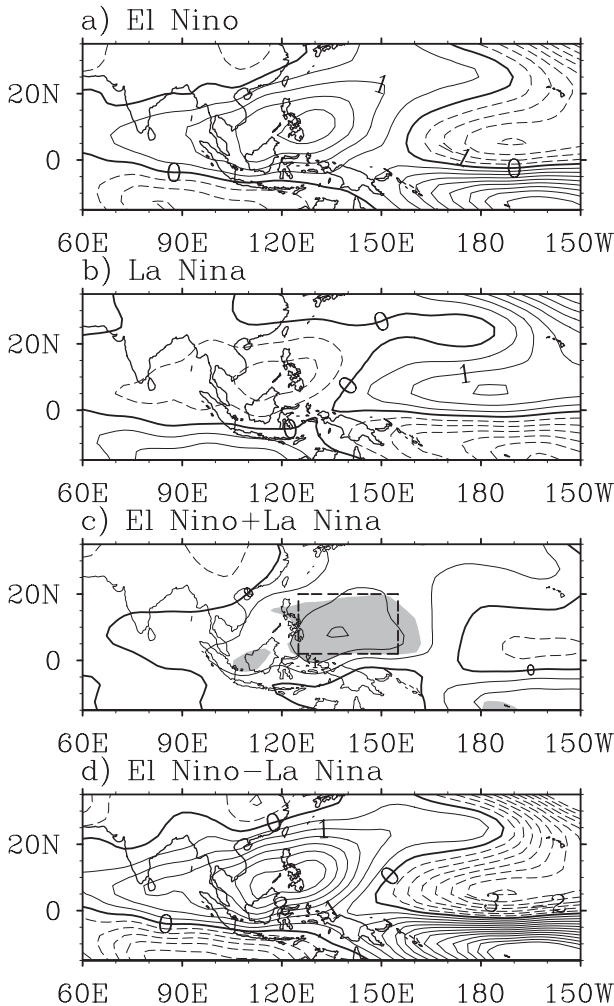


FIG. 1. Composite DJF mean 850-hPa streamfunction anomalies for (a) nine El Niño events and (b) nine La Niña events, listed in Table 1 (units: $10^6 \text{ m}^2 \text{ s}^{-1}$). (c) Asymmetric component estimated by the sum of (a) and (b). The shading represents the 10% significance level. (d) Symmetric component estimated by the difference of (a) and (b). Positive (solid lines) and negative values (dashed lines) are denoted; contour interval 0.5.

shift westward by 15° longitude with pronounced equatorial easterly anomalies extending to 135°E . As a result, the WNPC shifts westward relative to the WNPAC during El Niño, with a center located in the South China Sea (SCS).

The asymmetric component of the low-level circulations (Fig. 1c) is characterized by an anomalous anticyclone over the WNP, cyclone couplets over the equatorial central-eastern Pacific, and strong southwesterly winds from the Bay of Bengal to southeastern China. Note that the asymmetry between WNPAC and WNPC is the most significant feature in the asymmetric component of the low-level anomalous circulation fields between El Niño

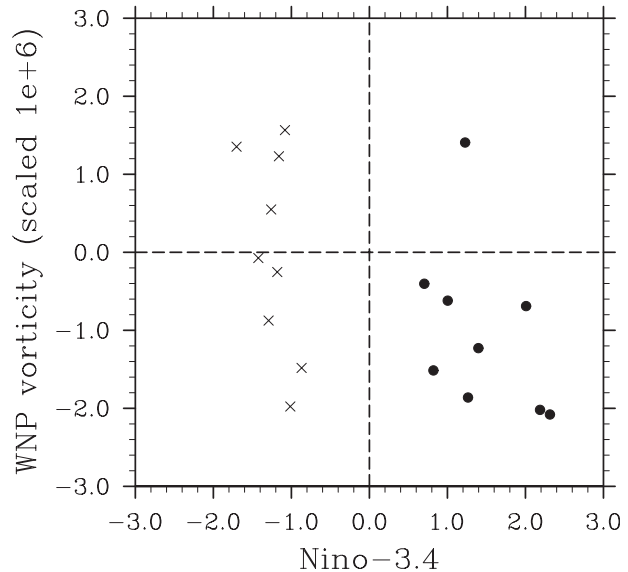


FIG. 2. Scatter diagram of the DJF mean Niño-3.4 index ($^\circ\text{C}$) vs the box-averaged vorticity anomalies over the western North Pacific ($2^\circ\text{--}20^\circ\text{N}$, $125^\circ\text{--}155^\circ\text{E}$, rectangular box in Fig. 1, units: 10^{-6} s^{-1}) for 18 ENSO events listed in Table 1: El Niño (dots) and La Niña (crosses) events.

and La Niña. In contrast, the symmetric component (Fig. 1d) represents the averaged condition of El Niño and La Niña, with an anticyclone located between the composite WNPAC and the composite WNPC.

As the maximum asymmetry of the 850-hPa streamfunction appears over the WNP ($2^\circ\text{--}20^\circ\text{N}$, $125^\circ\text{--}155^\circ\text{E}$; the rectangular box in Fig. 1c), we calculate the box-averaged vorticity for each event, shown as a scatter diagram in Fig. 2, together with corresponding Niño-3.4 indices. Nearly all El Niño events show negative vorticity anomalies over the WNP, except for the 1986 event. If the circulation anomalies were symmetric between El Niño and La Niña, we would expect positive vorticity anomalies during La Niña. However, only four out of nine La Niña events show positive vorticity anomalies. This asymmetry is consistent with the fact that the anomalous cyclones during most La Niña events shift westward away from the WNP. Figure 2 shows that there is no significant linear relationship between the amplitude of Niño-3.4 indices and the WNP vorticity. We explore the cause of the circulation asymmetry in next section.

4. Mechanisms responsible for the asymmetry between WNPAC and WNPC

The anomalous circulation over the WNP during the ENSO mature winter results from both local forcing of a negative SSTA in the WNP and remote forcing of a positive SSTA in the equatorial central-eastern Pacific

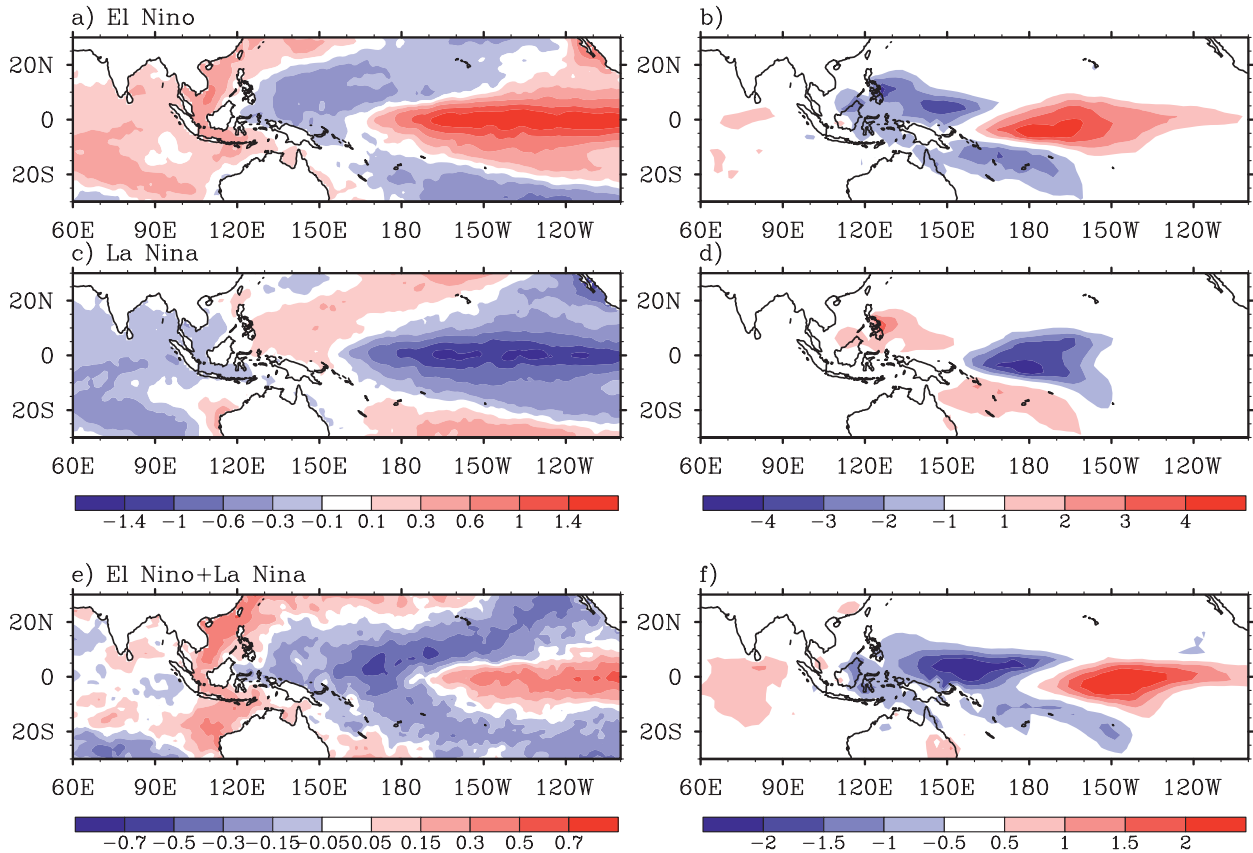


FIG. 3. As in Figs. 1a–c but for (a),(c),(e) SST anomalies ($^{\circ}\text{C}$) and (b),(d),(f) precipitation anomalies (mm day^{-1}).

(Wang et al. 2000; Lau and Nath 2000, 2003; Lau et al. 2004). To explore the asymmetric characteristics of the remote and local forcing between El Niño and La Niña, we show composite precipitation and SST anomalies and their asymmetric components in Fig. 3. Positive precipitation anomalies associated with El Niño extend from the equatorial central Pacific to the far eastern Pacific. In contrast, negative precipitation anomalies associated with La Niña are restricted to the west of 140°W and their center is located farther west, compared with the El Niño counterpart. Their asymmetric component exhibits a zonal dipole pattern, with a positive (negative) pole over the equatorial central-eastern (western) Pacific (Fig. 3f).

The SSTAs over the tropical central-eastern Pacific also present an asymmetric feature. The positive SSTAs in the tropical eastern Pacific during El Niño are stronger than the negative SSTAs during La Niña, whereas the negative SSTAs during La Niña are stronger in the tropical central Pacific and extend farther westward. As a result, the asymmetric component of the SSTAs also shows a zonal dipole pattern in the equatorial Pacific (Fig. 3e).

The above results imply that the asymmetry of the WNP circulation anomalies may be partially caused by the zonal asymmetries of the precipitation and SST anomalies between El Niño and La Niña. The anomalous SST and precipitation centers shift farther westward during La Niña. It is likely that the westward shift of the precipitation anomalies during La Niña causes the twin anomalous anticyclone couplets expanding into the tropical western Pacific. As a result, the center of the WNPC is pushed farther to the SCS (Fig. 1b).

To illustrate the effect of the zonal asymmetry of the anomalous precipitation center between El Niño and La Niña on the WNP circulations, a scatter diagram of the WNP vorticity versus the longitudinal location of the anomalous precipitation center over the equatorial central Pacific is shown in Fig. 4. Five out of nine El Niño events have positive convection centers located east of 170°W , while nearly all La Niña events have negative convection centers located near the date line. It is interesting to note that, when the precipitation centers are located to the east of 170°W , there is a close relationship between the sign of the WNP vorticity anomalies and the SSTA in the equatorial central-eastern Pacific; namely, an

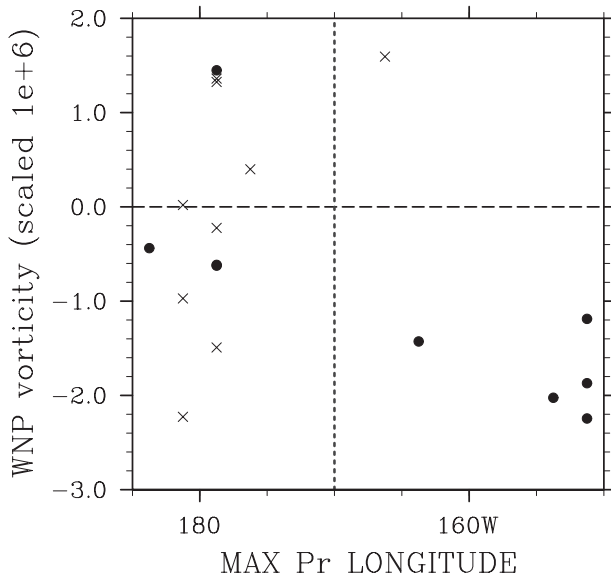


FIG. 4. Scatter diagram of the longitudinal location of the maximum amplitude of DJF mean 10°N – 10°S averaged precipitation anomalies over the Pacific vs the box-averaged vorticity anomalies over the western North Pacific (2° – 20°N , 125° – 155°E ; units: 10^{-6} s^{-1}) for 18 ENSO events, listed in Table 1: El Niño (dots) and La Niña (crosses) events.

anticyclone (cyclone) is associated with El Niño (La Niña). However, when the anomalous precipitation centers shift to the west of 170°W , the relationship becomes complicated, suggesting that some other factors rather than the longitudinal location of the heating must play active roles.

In addition to the equatorial east–west asymmetry, a significant asymmetry of SSTAs also appears in the off-equatorial WNP (Fig. 3e). The cold SSTAs in the WNP during El Niño are much stronger than the warm SSTAs during La Niña. Due to the weaker SSTAs, the precipitation anomalies over the WNP during La Niña are also much weaker than that during El Niño (Figs. 3b,d). There are two negative precipitation centers during El Niño, located at 15°N , 120°E and 5°N , 150°E , respectively (Fig. 3a). The former has a mirror image during La Niña, but the latter does not (Fig. 3b). It is crucial to understand why the asymmetric SSTAs, which cause asymmetric precipitation anomalies, emerge in the WNP.

To clearly illustrate the asymmetric evolution of the SSTAs in the WNP (Fig. 3e), we define a western North Pacific SST (WNPSST) index as the area-averaged SSTAs in the region 2° – 15°N , 130° – 155°E . Figure 5 shows the evolution of the WNPSST index during El Niño and La Niña. The WNPSST index reaches a peak phase in January, slightly lagging the mature phase of ENSO (Rasmusson and Carpenter 1982). It experiences two fast growing stages, one in June–August (JJA) and the

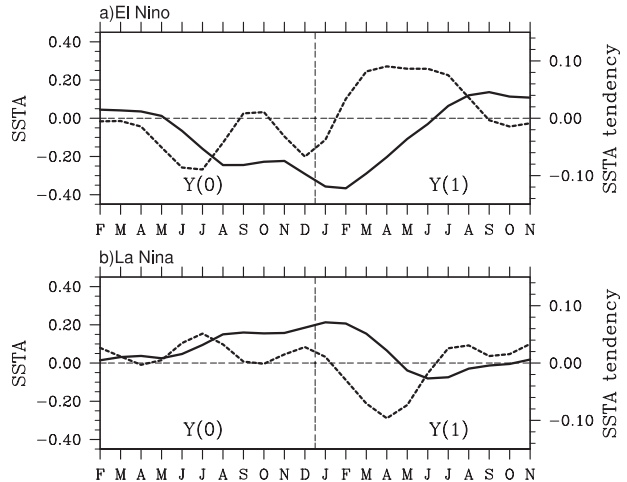


FIG. 5. Monthly mean time series (three-point smoother) of the WNPSST index, (solid line, $^{\circ}\text{C}$) and the temporal evolution of WNPSST tendency (dashed line, $^{\circ}\text{C month}^{-1}$) for the (a) El Niño and (b) La Niña composites. The WNPSST index is defined as box-averaged SST anomalies in the region 2° – 15°N , 130° – 155°E ; Y(0) and Y(1) represent ENSO-developing and ENSO-decaying years, respectively.

other in November–December (NDJ). During both stages, the absolute values of WNPSST index tendencies during El Niño are much larger than that during La Niña. Thus, the amplitude of the WNPSST in DJF during El Niño is about twice as large as that during La Niña.

Why does the WNPSST experience a stronger (weaker) growth during the El Niño (La Niña) development summer? To explore the possible mechanisms for the asymmetric evolutions of the WNPSST indices in JJA, we show composite SST, 1000-hPa wind, and precipitation anomalies during El Niño and La Niña in Fig. 6. Note that the warm SSTAs already have been established in the equatorial central-eastern Pacific during the El Niño development summer (Fig. 6b). The warm SSTAs enhance convection over the equatorial central Pacific (Fig. 6a), and thus stimulate twin low-level cyclone couplets in both sides of the equator, consistent with the classical Matsuno–Gill pattern (Matsuno 1966; Gill 1980). The northern branch of the cyclonic circulation anomalies is stronger than the southern one, which can be inferred from northward cross-equatorial flow anomalies over the Maritime Continent. The asymmetry is possibly attributed to the hemispheric asymmetry of the boreal summer mean flow such as the easterly vertical shear (Wang et al. 2003). The asymmetric flow over the Maritime Continent may be further enhanced by air–sea interaction in the tropical southeastern Indian Ocean (Li et al. 2002; Li et al. 2003; Wu et al. 2009).

The pattern of SSTAs during La Niña is generally symmetric with respect to that during El Niño (Fig. 6d).

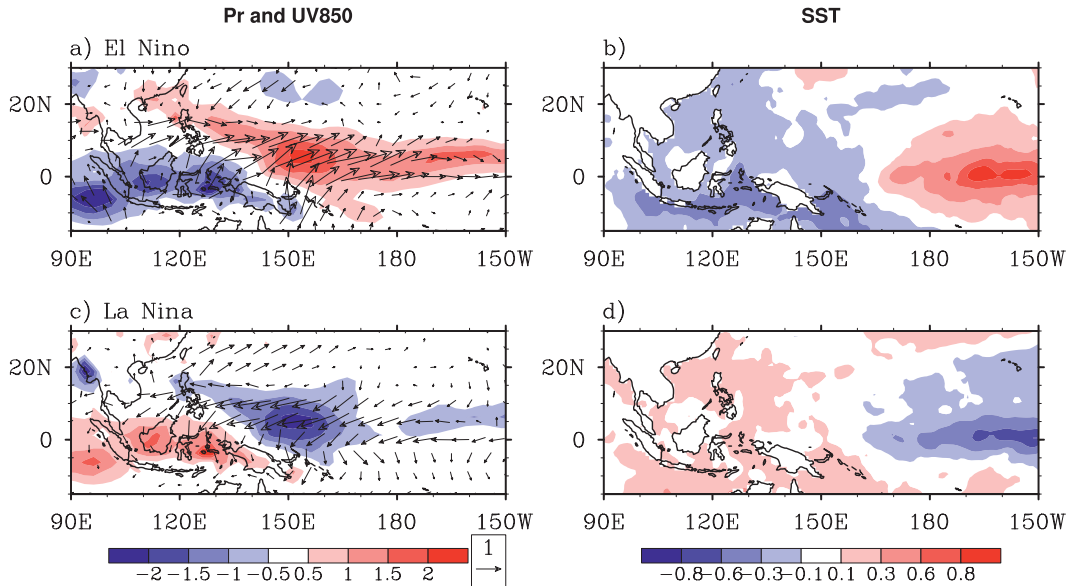


FIG. 6. Composite JJA mean 850-hPa wind anomalies (vector, units: $m s^{-1}$) and precipitation anomalies (shading, $mm day^{-1}$) for (a) El Niño and (c) La Niña events. Composite JJA mean SSTAs ($^{\circ}C$) for (b) El Niño and (d) La Niña events.

In particular, in the WNP, the amplitudes of the cold SSTAs during El Niño and the warm SSTAs during La Niña are quite close. Corresponding to the generally symmetric SSTA patterns, the precipitation and surface wind anomalies in the WNP between El Niño and La Niña are also quite symmetric (Figs. 6a,c).

Given the symmetric SST and wind patterns between El Niño and La Niña, a natural question that needs be addressed is what causes the asymmetric SSTA tendency in JJA. In the following we argue that the SSTA tendency asymmetry is primarily attributed to the asymmetry of the surface latent heat flux (LHF) anomaly. The LHF may be expressed as

$$LHF = \rho_0 L_v C_e U (Q_s - Q_a), \quad (1)$$

where ρ_0 , L_v , C_e , and U denote air density, the latent heat of vaporization, the surface exchange coefficient, and surface wind speed, respectively; Q_s is saturated specific humidity at SST and Q_a is air specific humidity at 10 m.

The anomalous surface wind speed and LHF fields during the El Niño- and La Niña-developing summers and their asymmetric components are shown in Fig. 7. The similarity of the patterns for anomalous wind and LHF suggests that the surface wind speed anomaly dominates the LHF anomaly in the WNP. Note that there is a large asymmetric component in the anomalous LHF field between El Niño and La Niña (Fig. 7f). The asymmetric LHF component is positive over the key region of the WNP (2°–15°N, 130°–155°E), implying a stronger

cooling (weaker warming) tendency in WNP during El Niño (La Niña).

Why are the anomalous surface wind speed and LHF fields greatly asymmetric in WNP, while the surface wind anomalies are quite symmetric in JJA between El Niño and La Niña (Figs. 6a,c)? Below we construct a simple ideal theoretical model to understand the nonlinear relationship between the LHF anomaly and the wind anomaly (Wang et al. 1999b).

Consider an idealized case in which only the mean and anomalous zonal winds are involved and the mean wind is westerly. Denote \bar{u} and u' as the magnitude of the mean and anomalous winds, and sps (spo) as the wind speed anomaly when the anomalous zonal wind is in the same (opposite) direction with the mean wind. Then, we have

$$sps = |\bar{u} + u'| - \bar{u} \quad (2)$$

and

$$spo = |\bar{u} - u'| - \bar{u}. \quad (3)$$

In the case when the amplitude of the mean wind is stronger than that of the anomalous wind (i.e., $\bar{u} > u'$), one may obtain a symmetric anomalous wind–wind speed relationship:

$$sps = u', \quad (4)$$

$$spo = -u'. \quad (5)$$

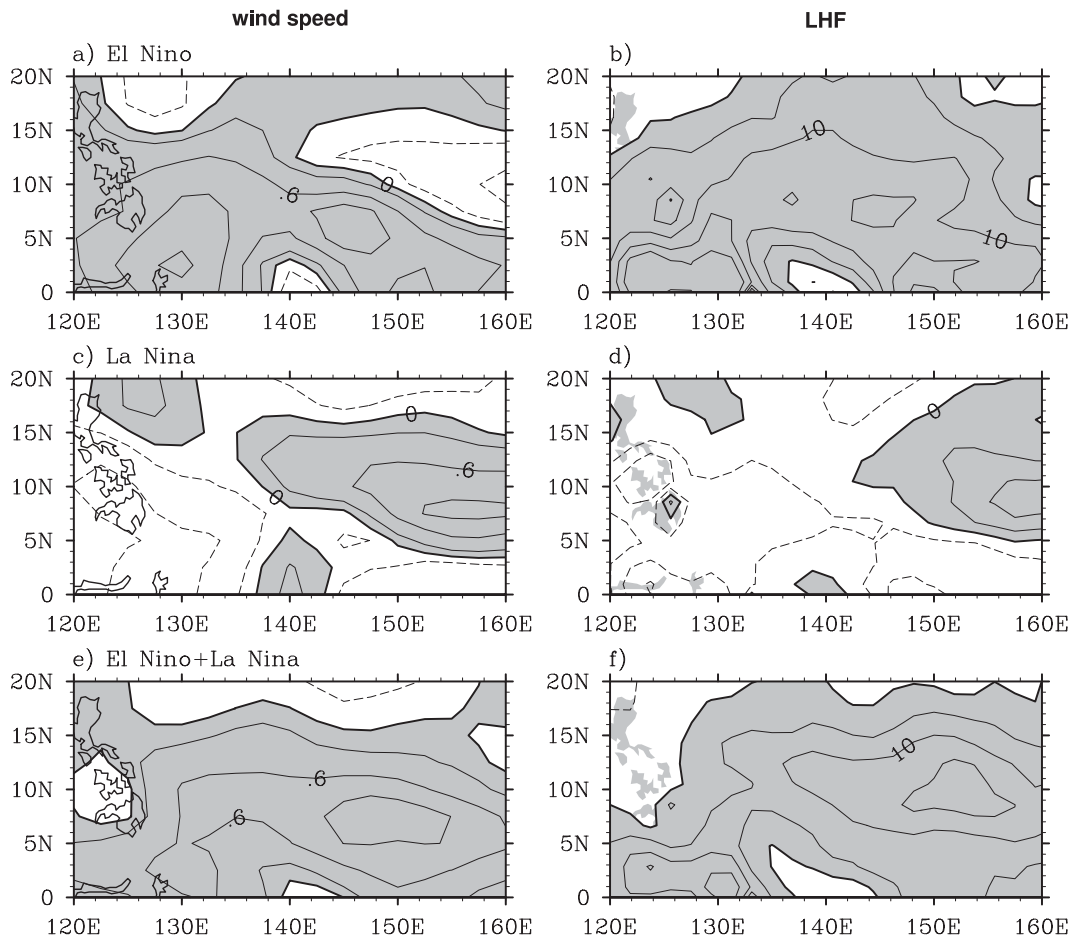


FIG. 7. Composite JJA mean 1000-hPa wind speed anomalies (m s^{-1}) for (a) El Niño and (c) La Niña events and (b),(d) corresponding latent heat flux anomalies (W m^{-2}). (e) Asymmetric component of the wind speed anomalies estimated by the sum of (a) and (c). (f) Asymmetric component of the latent heat flux anomalies estimated by the sum of (b) and (d).

In the case when the amplitude of the mean wind is weaker than that of the anomalous wind (i.e., $\bar{u} < u'$), one may obtain an asymmetric wind speed relationship as

$$\text{sps} = u', \quad (6)$$

and

$$\text{sps} = u' - 2\bar{u}. \quad (7)$$

Considering an extreme condition for which the mean wind is zero, the total wind speed would increase, no matter what direction the anomalous wind blows.

The theoretic model above indicates that there exist two dynamic regimes in the evaporation–wind feedback. The key difference between the two regimes lies in the relative amplitudes of the mean and anomalous winds. In the key region of the WNP (2° – 15°N , 130° – 155°E), the

amplitude of the anomalous zonal wind is about 3 m s^{-1} . However, the strength of the mean zonal wind is much smaller than 3 m s^{-1} in most of the region, except in the northeastern corner of the region (Fig. 8a). Area-averaged zonal wind in the region is about 0.7 m s^{-1} .

Figure 8b shows the theoretical model result based on the parameter values derived from the observation (i.e., the mean wind of 0.7 m s^{-1} and the anomalous wind amplitude of 3 m s^{-1}). When the anomalous wind is in the range from -0.7 to 0.7 m s^{-1} (i.e., weaker than the mean wind), resultant wind speed anomalies are symmetric. A westerly anomaly leads to a positive wind speed anomaly, whereas an easterly anomaly leads to a negative wind speed anomaly (Fig. 8b). When the anomalous wind is beyond the range of -0.7 to 0.7 m s^{-1} , resultant wind speed anomalies are asymmetric. Both strong westerly and easterly anomalies lead to a positive wind speed (and thus LHF) anomaly (Fig. 8b).

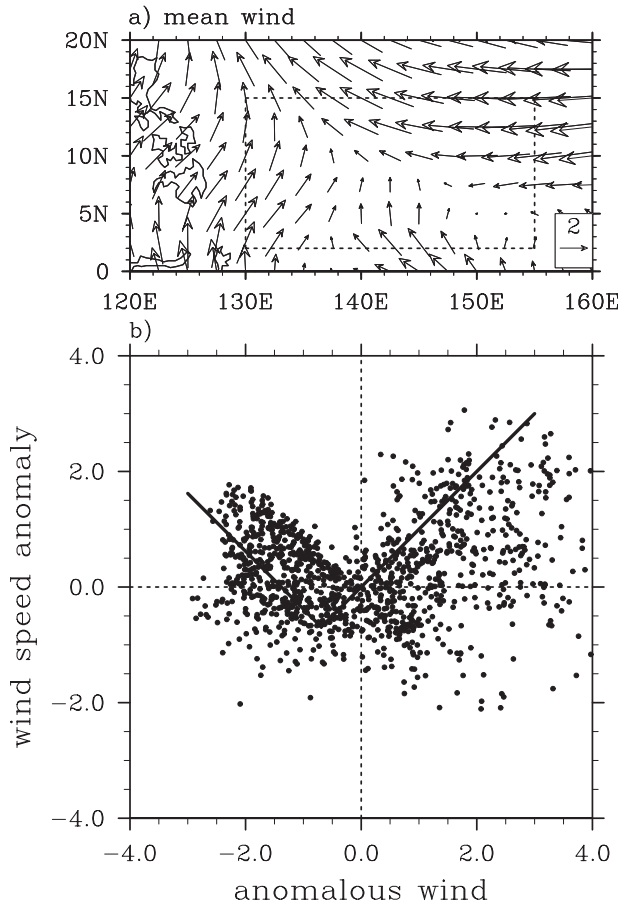


FIG. 8. (a) Climatological JJA mean 1000-hPa wind. The box represents the target region of the WNP (2° – 15° N, 130° – 155° E). (b) Scatter diagram of the JJA mean 1000-hPa zonal wind anomalies vs the 1000-hPa wind speed anomalies for each grid in the target region of WNP in 18 ENSO events. The thick line is calculated based on a theoretical model in which the mean wind is set to 0.7 m s^{-1} .

To compare the theoretical solution with real data, we show a scatter diagram of the zonal wind anomaly versus the wind speed anomaly for each grid in the WNP (2° – 15° N, 130° – 155° E; see Fig. 8b). As shown in Fig. 6, the anomalous winds in the region are dominated by their zonal component. Thus, we use the zonal wind anomalies to represent the total anomalous winds. The relationship between the zonal wind anomalies and wind speed anomalies is quite consistent with the theoretical model; that is, the enhancement of both positive and negative zonal wind anomalies during El Niño and La Niña leads to the increase of the wind speed and LHF anomalies. The positive LHF anomaly enhances the WNP SST cooling during El Niño but weakens the WNP SST warming during La Niña. Thus, the nonlinear relationship causes the asymmetry of the SST tendency in the WNP between El Niño and La Niña.

The analyses above indicate that the area 2° – 15° N, 130° – 155° E is a key region for generating asymmetric LHF anomalies between El Niño and La Niña during their development summer. It is located in a transitional zone between the monsoon westerly and the easterly trade wind, where the mean zonal wind is very weak (Fig. 8a). Even though the easterly anomalies during La Niña and the westerly anomalies during El Niño in JJA are approximately symmetric (Figs. 6a,c), the wind speed anomalies are enhanced in both cases. The asymmetry of LHF anomalies caused by the wind speed asymmetry may further induce the asymmetric SSTA tendencies in the WNP between El Niño and La Niña.

Another WNP SST tendency asymmetry between El Niño and La Niña occurs in NDJ (Fig. 5), which is primarily attributed to the asymmetry of anomalous wind fields. Note that in the WNP, the easterly anomaly appears in both El Niño and La Niña composites (Figs. 9a,b). The northeasterly anomaly over the WNP during El Niño connects the WNPAC to the west and a cyclonic circulation anomaly to the east (Fig. 9a). The former is a Rossby wave response to the local negative heating anomaly, whereas the latter is likely a Rossby wave response to the positive heating anomaly over the equatorial central Pacific. The easterly anomaly over the WNP during the La Niña, on the other hand, is the part of the anomalous circulation of the twin anticyclone couplet that is a direct response to the negative heating over the central equatorial Pacific (Fig. 9b). As the mean wind is northeasterly in the region, the anomalous wind would lead to an enhanced wind speed and LHF during both El Niño and La Niña (figure not shown). Correspondingly, the asymmetric components of the surface wind speed and the LHF anomalies are positive in the WNP region (2° – 15° N, 130° – 155° E; see Fig. 9c). The asymmetry of LHF anomalies leads to an enhanced cooling during El Niño but a reduced warming during La Niña in this region. As a result, the asymmetry of the WNP SSTAs between El Niño and La Niña becomes even greater, leading to a more significant difference between the WNPAC and the WNPC.

5. The results of AGCM experiments

Observational analyses above suggest that both asymmetries of the remote forcing from the tropical central Pacific and the local SST forcing in the WNP may cause the asymmetry between WNPAC and WNPC. In this section we examine their relative roles by analyzing the results of the numerical experiments listed in Table 2.

The GB experiment is analyzed first to test the basic model skill in reproducing the asymmetry between WNPAC and WNPC during the ENSO mature winter

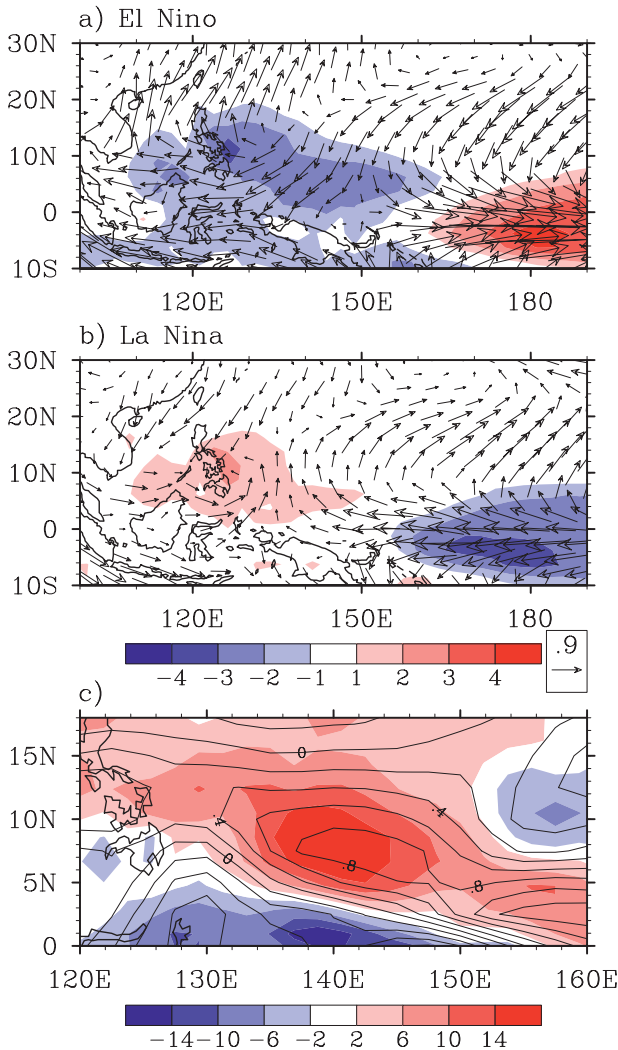


FIG. 9. (a) El Niño and (b) La Niña composite NDJ mean 1000-hPa wind anomalies (vectors, m s^{-1}) and precipitation anomalies (contours, mm day^{-1}). (c) Asymmetric components of 1000-hPa wind speed anomalies (contours, m s^{-1}) and latent heat flux anomalies (shading, W m^{-2}) between El Niño and La Niña.

(DJF). The simulated precipitation and 850-hPa wind anomalies in the GBEL and GBLA runs and their asymmetric components are shown in Fig. 10. The anomalies are calculated as departures from the CTRL run. The simulated circulation and precipitation anomalies can be compared against Fig. 1 and the right panel of Fig. 3, respectively. The GB experiment reproduces the WNPAC (WNPC) during El Niño (La Niña) and corresponding negative (positive) precipitation anomalies over the WNP and positive (negative) precipitation anomalies over the equatorial central Pacific. The model reproduces the major asymmetric characteristic between the WNPAC and WNPC; that is, the WNPC is much weaker than the WNPAC and is located farther to the west of the

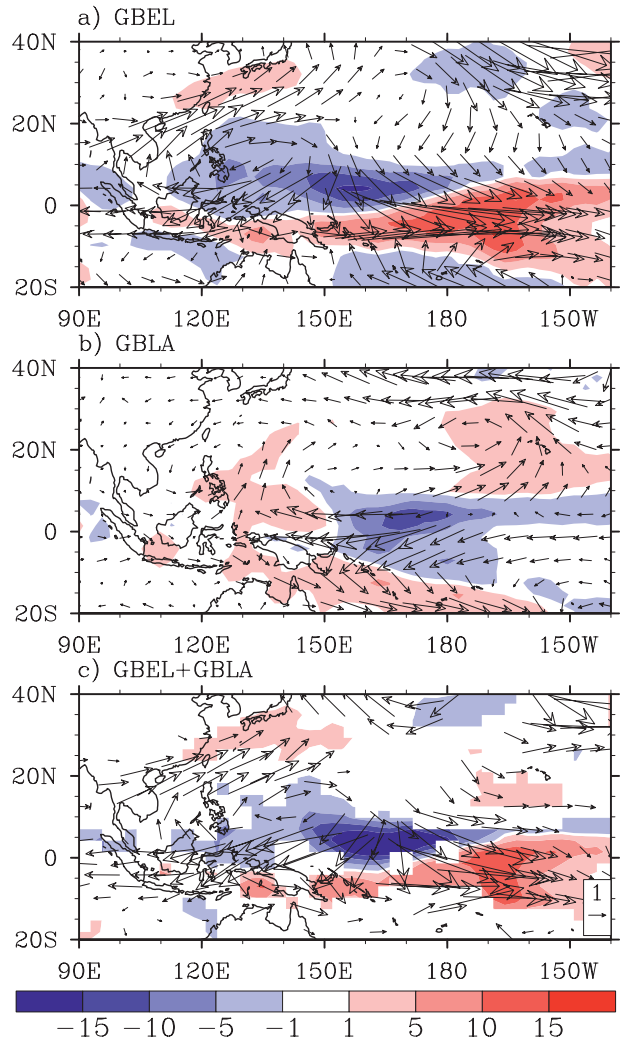


FIG. 10. (a) Difference of the precipitation (shading, mm day^{-1}) and 850-hPa wind (vectors, m s^{-1}) fields in DJF between the GBEL and CTRL runs. (b) Same as (a), but for the GBLA runs. (c) Asymmetric component of (a) and (b), estimated by their sum; only values in the 10% significance level are shown.

WNPAC. It should be noted that the simulated asymmetric component between WNPAC and WNPC is much larger than that in the observation, owing to the weaker WNPC in the GBLA runs. The model reproduces well the zonal shift of the anomalous heating over the equatorial central Pacific and the strength difference of the anomalous heating over the WNP, indicating that it is capable of capturing the impacts of both remote central-eastern Pacific and local WNP SST forcing. The results give us confidence to further explore their relative roles through sensitive experiments.

The precipitation and 850-hPa wind anomalies simulated by the CEEL and CELA runs and their asymmetric components are shown in Figs. 11a–c. The CEEL

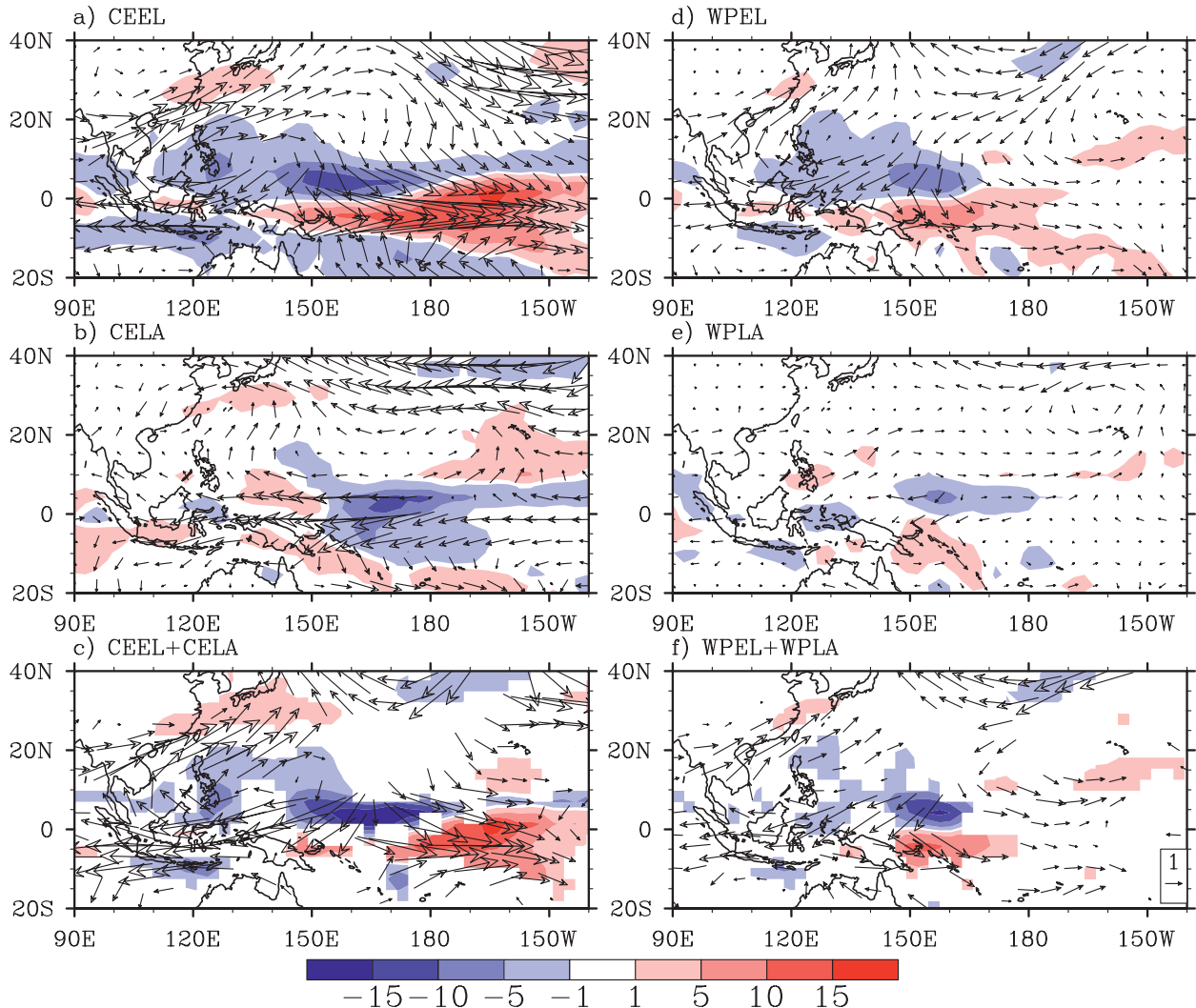


FIG. 11. As in Fig. 10 but for the (a)–(c) CEEL and CELA runs and (d)–(f) WPEL and WPLA runs.

(CELA) reproduces the WNPAC (WNPC) and the corresponding negative (positive) precipitation anomalies over the WNP and positive (negative) precipitation anomalies over the equatorial central Pacific, though some biases exist. Compared with the GBEL runs, the WNPAC simulated by the CEEL runs shifts westward to some extent, and the negative precipitation anomalies over the WNP are weaker, especially in the region of 130°–140°E. The differences between CELA and GBLA are larger. The easterly anomalies induced by the negative heating over the equatorial central Pacific extend into the Maritime Continent. The WNPC shifts farther northward. The differences occur because of the lack of local forcing in the WNP. In summary, the asymmetry between the WNPAC and WNPC generally can be reproduced in the CE experiments, although the center of the asymmetric component shifts westward relative to the GB experiments.

The results of the WP experiments are shown in Figs. 11d–f. The WNPAC is reproduced, but with amplitudes far weaker than their counterparts in the CEEL runs. In the CELA runs, the WNPC is weakly simulated, with weak westerlies seen in the WNP. However, compared with the CE experiments, the locations of the WNPAC in the CEEL runs and the WNP westerly anomalies in the CELA runs are closer to those in the GB experiments. The asymmetry of the WNP circulation anomalies is also reproduced by the WP experiments, though the asymmetric component is weaker than that in the GB and CE experiments.

The model results support our hypothesis based on observational diagnosis that both of the asymmetries of the remote forcing from the equatorial central-eastern Pacific and the local SSTA forcing in the WNP contribute to the asymmetry between the WNPAC and WNPC. The

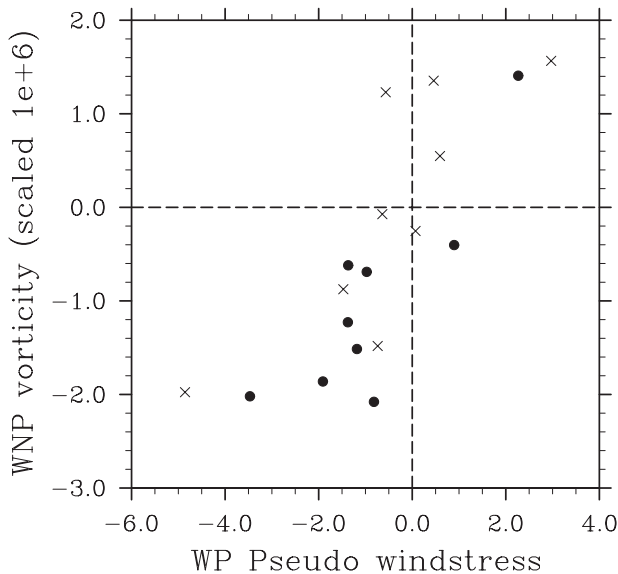


FIG. 12. Scatter diagram of the DJF mean box-averaged zonal pseudo-wind stress anomalies over the equatorial western Pacific (5°N – 5°S , 125° – 155°E) vs the box-averaged 850-hPa vorticity anomalies over the western North Pacific (2° – 20°N , 125° – 155°E) for ENSO events, listed in Table 1: El Niño (dots) and La Niña (crosses) events.

numerical experiments demonstrate that the remote forcing from the equatorial central-eastern Pacific play greater roles than the local WNP SST.

6. Impact of the asymmetry on ENSO phase reversal

Previous studies noted the essential role of equatorial zonal wind stress over the equatorial western Pacific in ENSO phase reversal (Weisberg and Wang 1997a,b; Kim and Lau 2001; Lau and Wu 2001; Kug and Kang 2006). To investigate relationship between the WNPC/WNPAC and the zonal wind stress anomalies over the equatorial western Pacific, we show the scatter diagram of the box-averaged zonal pseudo-wind stress anomalies over the equatorial western Pacific (5°S – 5°N , 125° – 155°E) versus 850-hPa vorticity anomalies over the WNP (2° – 20°N , 125° – 155°E ; see Fig. 12). Their correlation coefficient reaches 0.79, which is statistically significant at the 1% level, indicating that the WNP vorticity accounts for about half of the variance of the zonal wind stress over the equatorial western Pacific during the ENSO mature winter.

The easterly wind stress anomalies prevail during seven out of nine El Niño events, except for the 1986 and 1994 events. In contrast, only three La Niña events have westerly wind stress anomalies at the equator. Some La Niña events even have strong equatorial easterly wind stress anomalies.

The asymmetry of the equatorial wind stress anomalies over the western Pacific is likely responsible for the asymmetry of ENSO evolution (Ohba and Ueda 2009). Figure 13 shows that following the El Niño and La Niña peak phase in boreal winter, canonical El Niño experiences a fast decay and translates to a negative phase in boreal summer. In contrast, La Niña tends to persist through the next year. To quantify the decaying rate of the Niño-3.4 index, we calculated the tendency of the Niño-3.4 indices of composite El Niño and La Niña, respectively (Fig. 13). Both El Niño and La Niña reach the fastest decaying rate in March, with the former being much larger than the latter. In addition, El Niño tends to keep the strong decay rate much longer than La Niña. As an exception, the 1986 El Niño does not decay after DJF and is maintained until the 1988 summer.

To show the different evolutionary characteristics of oceanic subsurface during El Niño and La Niña under asymmetric forcing of the equatorial zonal wind stress anomalies over the western Pacific, we show the temporal evolution of composite 20°C isotherm depth anomalies along the equator (Fig. 14). The change of the subsurface temperature is primarily caused by the thermocline variation, which is intimately linked to the passage of Kelvin waves. In September, two months before the ENSO mature phase, the 20°C isotherms in the western Pacific during El Niño and La Niña are both close to the climatological state. In December, after the formation of the WNPAC and the associated equatorial easterly wind stress anomalies over the western Pacific, the underlying thermocline during El Niño significantly rises (Fig. 14a), and the subsurface temperature in the equatorial western Pacific decreases (figure not shown). In contrast, the amplitude of the thermocline depth anomalies during La Niña changes much less (Fig. 14b). In the course of eastward propagation, the upwelling Kelvin waves during El Niño are persistently stronger than the downwelling Kelvin waves during La Niña. Thus, El Niño decays much more quickly than La Niña.

7. Summary and concluding remarks

This paper deals with the asymmetry of the WNP atmospheric circulation anomalies between the El Niño and La Niña mature winter. The physical mechanisms responsible for the asymmetry are studied from two plausible aspects: the intrinsic asymmetries of ENSO remote forcing and local air–sea interaction. Both processes are demonstrated with idealized numerical experiments. The impacts of the asymmetry on the ENSO phase reversal are also investigated. The major findings are summarized below.

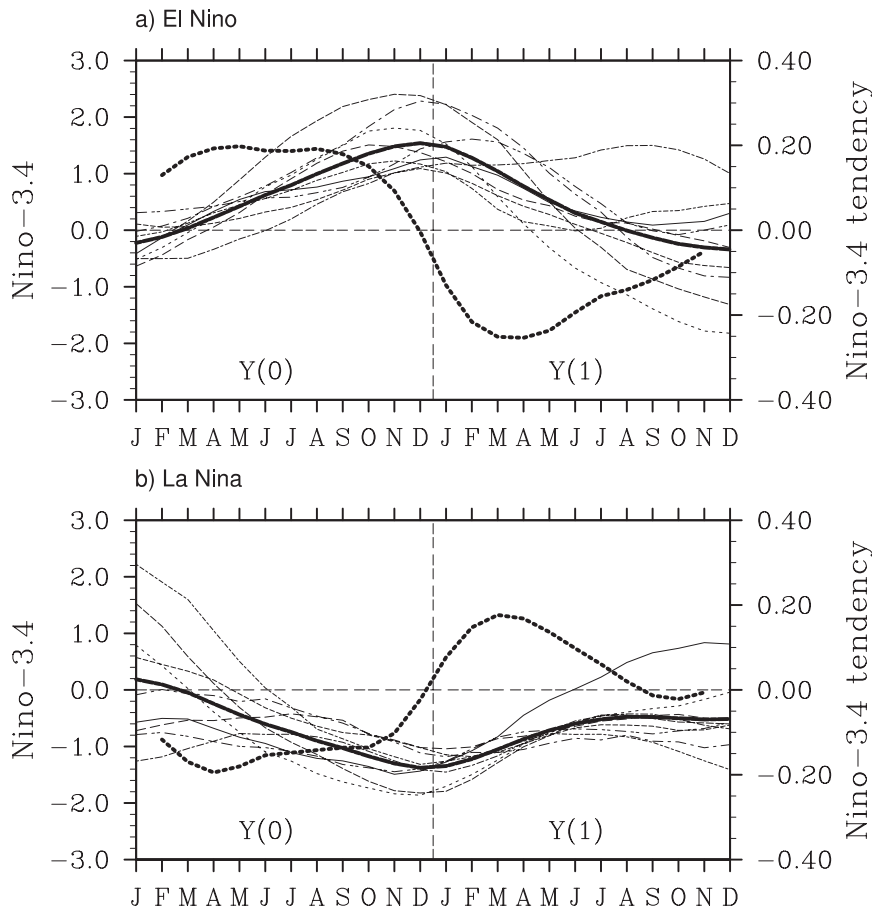


FIG. 13. Temporal evolution of monthly mean Niño-3.4 (5°S–5°N, 190°–240°E) SST anomalies (°C) from January of the ENSO development year to December of the following year for (a) El Niño and (b) La Niña events (thin lines). Composite Niño-3.4 SST anomalies (solid thick line) and the SSTAs tendency (dashed thick line) are also shown. Niño-3.4 indices are filtered by a five-point smoother. Y(0) and Y(1) indicate the ENSO-development year and decay years, respectively.

- The WNPC during La Niña tends to shift westward relative to the WNPAC during El Niño. While the WNPAC center is located over the Philippine Sea, the WNPC center is located over the SCS. Correspondingly, equatorial westerly anomalies in the southern flank of the WNPC withdraw westward about 20° relative to their El Niño counterparts.
- Two possible mechanisms responsible for the phase shift are examined. First, as a Rossby wave response to the negative heating over the equatorial central Pacific, twin anticyclone couplets during La Niña shift westward relative to twin cyclone couplets during El Niño due to the spatial phase shift of SST and precipitation anomalies over the equatorial central Pacific. Second, the intensities of negative SSTAs and associated negative precipitation anomalies in the WNP during El Niño are stronger than the La Niña counterparts.

The asymmetry of the SSTAs arises from asymmetric SSTA tendency in JJA and NDJ.

- In JJA, though SSTAs, precipitation, and wind anomalies are generally symmetric between El Niño and La Niña (i.e., a mirror image), surface wind speed anomalies and corresponding latent heat flux are highly asymmetric. The asymmetric latent heat flux further causes the asymmetric SSTA tendency. In NDJ, the asymmetric SSTA tendency is primarily attributed to the asymmetry of anomalous wind fields between El Niño and La Niña; the WNP is covered by easterly anomalies during both El Niño and La Niña. The easterly anomalies would enhance surface wind speed and latent heat flux. As a result, the asymmetry of the local SSTAs between El Niño and La Niña is further amplified.
- Two distinctive wind–evaporation feedback regimes are identified to explain the asymmetry of the latent

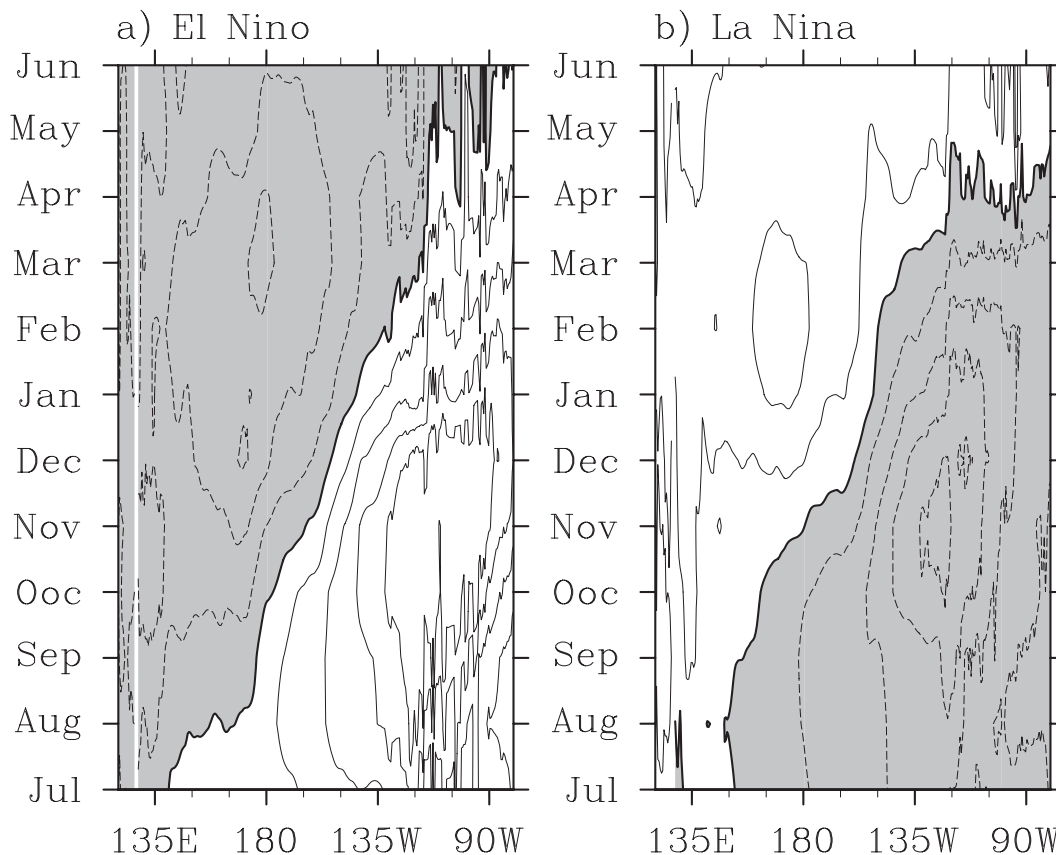


FIG. 14. Time-longitude distributions of 20°C isotherm anomalies (m) averaged over 2°N – 2°S for the (a) El Niño composite and (b) La Niña composite [July(0)-June(1)]. The data are derived from the SODA reanalysis. Contour interval is 8; negative values are shaded.

heat flux anomaly during the ENSO development summer (JJA). Since the wind speed anomalies are determined by both anomalous wind and background mean wind, when the mean wind is stronger (weaker) than the anomalous wind, wind speed anomalies are symmetric (asymmetric) with respect to the opposite anomalous winds. Therefore, the wind speed anomalies exhibit dominant asymmetric characteristics between El Niño and La Niña in the transitional zone between the monsoon westerly and the trade easterly, where the mean wind is very weak. The asymmetry of the wind speed anomalies further cause the asymmetry of the latent heat flux anomalies.

- The hypotheses based on data diagnosis are further confirmed by the results of numerical experiments, which indicate that both the asymmetries of the remote forcing from the equatorial central Pacific and the local SSTA forcing in the WNP contribute to the asymmetry between the WNPAC and WNPC. The impact of the former is larger than the latter in terms of the amplitudes of model responses.

- Due to the westward shift of the WNPC center, westerly wind stress anomalies over the equatorial western Pacific during the La Niña mature phase are much weaker than easterly wind stress anomalies during El Niño. The weak (strong) wind stress anomalies during La Niña (El Niño) may stimulate weak (strong) oceanic Kelvin waves, leading to a slower (faster) phase transition to El Niño (La Niña). This may partially explain the evolution asymmetry between El Niño and La Niña.

It should be noted that, in this study, we focus on the asymmetry of the WNP circulation anomalies between El Niño and La Niña, but pay less attention to the non-linearity between El Niño and La Niña events. For instance, the 1986 winter is an El Niño winter during which the WNP is covered by an anomalous cyclone, instead of an anomalous anticyclone. The SSTAs in the equatorial eastern Pacific did not decay after the winter, but persisted through the next year. The cause of this special event is not clear at present and warrants further studies.

While the endeavor in this regard has been puzzling owing to the limitation of sample size, a long-term coupled model simulation may help us to understand the issue.

In addition, we only focus on the tropical processes in our analysis above. It was found that during the fall of El Niño events, the East Asian trough deepens, which may enhance cold air outbreaks and initiate the WNPAC (Wang and Zhang 2002). In fact, by checking the composite maps for the September–October mean 500-hPa geopotential height anomalies for El Niño and La Niña, we note that the deepening of the East Asian trough during El Niño is much stronger than the shoaling of the trough during La Niña. This asymmetric characteristic may also contribute to the asymmetry between the WNPAC and WNPC. More detailed analysis of this midlatitude impact is needed in future work.

Acknowledgments. This work was supported by NSFC Grants 40628006, 40821092, and 40523001, the National Basic Research Program of China (2006CB403603), RandD Special Fund for Public Welfare Industry (meteorology; GYHY200706010, GYHY200806010). TL was supported by ONR Grants N000140710145 and N000140810256 and by the International Pacific Research Center, which is sponsored by the Japan Agency for Marine–Earth Science and Technology (JAMSTEC), NASA (NNX07AG53G), and NOAA (NA17RJ1230).

REFERENCES

- An, S.-I., and F.-F. Jin, 2004: Nonlinearity and asymmetry of ENSO. *J. Climate*, **17**, 2399–2412.
- , Y. G. Ham, J. S. Kug, F. F. Jin, and I. S. Kang, 2005: El Niño–La Niña asymmetry in the Coupled Model Intercomparison Project simulations. *J. Climate*, **18**, 2617–2627.
- Burgers, G., and D. B. Stephenson, 1999: The normality of El Niño. *Geophys. Res. Lett.*, **26**, 1027–1030.
- Carton, J. A., G. Chepurin, and X. H. Cao, 2000: A Simple Ocean Data Assimilation analysis of the global upper ocean 1950–95. Part II: Results. *J. Phys. Oceanogr.*, **30**, 311–326.
- Chang, C. P., Y. S. Zhang, and T. Li, 2000a: Interannual and interdecadal variations of the East Asian summer monsoon and tropical Pacific SSTs. Part I: Roles of the subtropical ridge. *J. Climate*, **13**, 4310–4325.
- , —, and —, 2000b: Interannual and interdecadal variations of the East Asian summer monsoon and tropical Pacific SSTs. Part II: Meridional structure of the monsoon. *J. Climate*, **13**, 4326–4340.
- Chang, P., J. Li, and H. Li, 1997: A decadal climate variation in the tropical Atlantic Ocean from thermodynamic air–sea interactions. *Nature*, **385**, 516–518.
- Chen, J. M., T. Li, and C. F. Shih, 2007: Fall persistence barrier of sea surface temperature in the South China Sea associated with ENSO. *J. Climate*, **20**, 158–172.
- Chen, M., P. Xie, J. E. Janowiak, and P. A. Arkin, 2002: Global land precipitation: A 50-yr monthly analysis based on gauge observations. *J. Hydrometeorol.*, **3**, 249–266.
- Chou, C., 2004: Establishment of the low-level wind anomalies over the western North Pacific during ENSO development. *J. Climate*, **17**, 2195–2212.
- Duchon, C., 1979: Lanczos filtering in one and two dimensions. *J. Appl. Meteor.*, **18**, 1016–1022.
- Gill, A. E., 1980: Some simple solutions for heat-induced tropical circulation. *Quart. J. Roy. Meteor. Soc.*, **106**, 447–462.
- Hoerling, M. P., A. Kumar, and M. Zhong, 1997: El Niño, La Niña, and the nonlinearity of their teleconnections. *J. Climate*, **10**, 1769–1786.
- Jin, F.-F., S.-I. An, A. Timmermann, and J. Zhao, 2003: Strong El Niño events and nonlinear dynamical heating. *Geophys. Res. Lett.*, **30**, 1120, doi:10.1029/2002GL016356.
- Kalnay, E., and Coauthors, 1996: The NCEP/NCAR 40-Year Reanalysis Project. *Bull. Amer. Meteor. Soc.*, **77**, 437–471.
- Kang, I.-S., and J.-S. Kug, 2002: El Niño and La Niña sea surface temperature anomalies: Asymmetry characteristics associated with their wind stress anomalies. *J. Geophys. Res.*, **107**, 4372, doi:10.1029/2001JD000393.
- Kim, K. M., and K. M. Lau, 2001: Dynamics of monsoon-induced biennial variability in ENSO. *Geophys. Res. Lett.*, **28**, 315–318.
- Kug, J.-S., and I.-S. Kang, 2006: Interactive feedback between ENSO and the Indian Ocean. *J. Climate*, **19**, 1784–1801.
- Lau, K. M., and H. T. Wu, 2001: Principal modes of rainfall–SST variability of the Asian summer monsoon: A reassessment of monsoon–ENSO relationship. *J. Climate*, **14**, 2880–2895.
- Lau, N.-C., and M. J. Nath, 2000: Impact of ENSO on the variability of the Asian–Australian monsoons as simulated in GCM experiments. *J. Climate*, **13**, 4287–4309.
- , and —, 2003: Atmosphere–ocean variations in the Indo-Pacific sector during ENSO episodes. *J. Climate*, **16**, 3–20.
- , and —, 2006: ENSO modulation of the interannual and intraseasonal variability of the East Asian monsoon—A model study. *J. Climate*, **19**, 4508–4530.
- , and H. Wang, 2004: Simulations by a GFDL GCM of ENSO-related variability of the coupled atmosphere–ocean system in the East Asian monsoon region. *East Asian Monsoon*, C.-P. Chang, Ed., World Scientific Series on Meteorology of East Asia, Vol. 2, World Scientific, 271–300.
- Li, T., 1997: Air–sea interactions of relevance to the ITCZ: The analysis of coupled instabilities and experiments in a hybrid coupled GCM. *J. Atmos. Sci.*, **54**, 134–147.
- , Y. S. Zhang, E. Lu, and D. Wang, 2002: Relative role of dynamic and thermodynamic processes in the development of the Indian Ocean dipole. *Geophys. Res. Lett.*, **29**, 2110, doi:10.1029/2002GL015789.
- , B. Wang, C. P. Chang, and Y. S. Zhang, 2003: A theory for the Indian Ocean dipole-zonal mode. *J. Atmos. Sci.*, **60**, 2119–2135.
- Li, Y., R. Lu, and B. Dong, 2007: The ENSO–Asian monsoon interaction in a coupled ocean–atmosphere GCM. *J. Climate*, **20**, 5164–5177.
- Matsuno, T., 1966: Quasi-geostrophic motions in the equatorial area. *J. Meteor. Soc. Japan*, **44**, 25–42.
- Ohba, M., and H. Ueda, 2009: Role of nonlinear atmospheric response to SST on the asymmetric transition process of ENSO. *J. Climate*, **22**, 177–192.
- Rasmusson, E. M., and T. H. Carpenter, 1982: Variations in tropical sea surface temperature and surface wind fields associated with the Southern Oscillation/El Niño. *Mon. Wea. Rev.*, **110**, 554–584.
- Rayner, N. A., D. E. Parker, E. B. Horton, C. K. Folland, L. V. Alexander, D. P. Rowell, E. C. Kent, and A. Kaplan, 2003: Global analyses of sea surface temperature, sea ice, and

- night marine air temperature since the late nineteenth century. *J. Geophys. Res.*, **108**, 4407, doi:10.1029/2002JD002670.
- Roeckner, E., and Coauthors, 1996: The atmospheric general circulation model ECHAM-4: Model description and simulation of present-day climate. Max-Planck-Institute for Meteorology Rep. 218, 90 pp. [Available online at http://www.mpimet.mpg.de/fileadmin/publikationen/Reports/MPI-Report_218.pdf.]
- Sui, C.-H., P.-H. Chung, and T. Li, 2007: Interannual and interdecadal variability of the summertime western North Pacific subtropical high. *Geophys. Res. Lett.*, **34**, L11701, doi:10.1029/2006GL029204.
- Wang, B., and Q. Zhang, 2002: Pacific–east Asian teleconnection. Part II: How the Philippine Sea anomalous anticyclone is established during El Niño development. *J. Climate*, **15**, 3252–3265.
- , R. G. Wu, and X. H. Fu, 2000: Pacific–East Asian teleconnection: How does ENSO affect East Asian climate? *J. Climate*, **13**, 1517–1536.
- , —, R. Lukas, and S. I. An, 2001: A possible mechanism for ENSO turnabout. *Dynamics of Atmospheric General Circulation and Climate*, IAP/Academia Sinica, Ed., China Meteorological Press, 552–578.
- , —, and T. Li, 2003: Atmosphere–warm ocean interaction and its impacts on Asian–Australian monsoon variation. *J. Climate*, **16**, 1195–1211.
- Wang, C. Z., R. H. Weisberg, and J. I. Virmani, 1999a: Western Pacific interannual variability associated with the El Niño–Southern Oscillation. *J. Geophys. Res.*, **104**, 5131–5149.
- , —, and H. J. Yang, 1999b: Effects of the wind speed–evaporation–SST feedback on the El Niño–Southern Oscillation. *J. Atmos. Sci.*, **56**, 1391–1403.
- Weisberg, R. H., and C. Z. Wang, 1997a: A western Pacific oscillator paradigm for the El Niño Southern Oscillation. *Geophys. Res. Lett.*, **24**, 779–782.
- , and —, 1997b: Slow variability in the equatorial west-central Pacific in relation to ENSO. *J. Climate*, **10**, 1998–2017.
- Wu, B., and T. J. Zhou, 2008: Oceanic origin of the interannual and interdecadal variability of the summertime western Pacific subtropical high. *Geophys. Res. Lett.*, **35**, L13701, doi:10.1029/2008GL034584.
- , —, and T. Li, 2009: Contrast of rainfall–SST relationships in the western North Pacific between the ENSO developing and decaying summers. *J. Climate*, **16**, 4398–4405.
- Wu, R., Z.-Z. Hu, and B. P. Kirtman, 2003: Evolution of ENSO-related rainfall anomalies in East Asia. *J. Climate*, **16**, 3742–3758.
- Xie, S.-P., 1999: A dynamic ocean–atmosphere model of the tropical Atlantic decadal variability. *J. Climate*, **12**, 64–70.
- , and S. G. H. Philander, 1994: A coupled ocean–atmosphere model of relevance to the ITCZ in the eastern Pacific. *Tellus*, **46A**, 340–350.
- Zhang, R. H., and A. Sumi, 2002: Moisture circulation over East Asia during El Niño episode in northern winter, spring and autumn. *J. Meteor. Soc. Japan*, **80**, 213–227.
- , —, and M. Kimoto, 1996: Impact of El Niño on the East Asian monsoon: A diagnostic study of the '86/87 and '91/92 events. *J. Meteor. Soc. Japan*, **74**, 49–62.
- Zhou, T. J., and R. C. Yu, 2005: Atmospheric water vapor transport associated with typical anomalous summer rainfall patterns in China. *J. Geophys. Res.*, **110**, D08104, doi:10.1029/2004JD005413.
- , B. Wu, and B. Wang, 2009a: How well do atmospheric general circulation models capture the leading modes of the interannual variability of Asian–Australian monsoon? *J. Climate*, **22**, 1159–1173.
- , and Coauthors, 2009b: Why the western Pacific subtropical high has extended westward since the late 1970s. *J. Climate*, **22**, 2199–2215.